

Block-Activated Algorithms for Multicomponent Fully Nonsmooth Minimization*

Minh N. Bùi, Patrick L. Combettes, and Zev C. Woodstock

North Carolina State University, Department of Mathematics, Raleigh, NC 27695-8205, USA
mnbui@ncsu.edu, plc@math.ncsu.edu, zwoodst@ncsu.edu

Abstract. We investigate block-activated proximal algorithms for multicomponent minimization problems involving a separable nonsmooth convex function penalizing the components individually, and nonsmooth convex coupling terms penalizing linear mixtures of the components. In the case of smooth coupling functions, several algorithms exist and they are well understood. By contrast, in the fully nonsmooth case, few block-activated methods are available and little effort has been devoted to assessing their merits and numerical performance. The goal of the paper is to address this gap. The numerical experiments concern machine learning and signal recovery problems.

Keywords. Block-activation, image recovery, machine learning, convex optimization, nonsmooth minimization, proximal splitting.

*The work of M. N. Bùi and P. L. Combettes was supported by the National Science Foundation under grant CCF-1715671 and the work of Z. C. Woodstock was supported by the National Science Foundation under grant DGE-1746939.

1 Introduction

The goal of many signal processing and machine learning tasks is to exploit the observed data and the prior knowledge to produce a solution that represents information of interest. In this process of extracting information from data, structured convex optimization has established itself as an effective modeling and algorithmic framework; see for instance [3, 5, 9, 15, 19]. In state-of-the-art applications, the sought solution is often a tuple of vectors which reside in different spaces [1, 2, 6, 7, 13, 14, 17]. The following multicomponent minimization problem will be shown to capture a wide range of concrete scenarios. It consists of a separable term penalizing the components individually, and of coupling terms penalizing linear mixtures of the components.

Problem 1 Let $(\mathcal{H}_i)_{1 \leq i \leq m}$ and $(\mathcal{G}_k)_{1 \leq k \leq p}$ be Euclidean spaces. For every $i \in \{1, \dots, m\}$ and every $k \in \{1, \dots, p\}$, let $f_i: \mathcal{H}_i \rightarrow]-\infty, +\infty]$ and $g_k: \mathcal{G}_k \rightarrow]-\infty, +\infty]$ be proper lower semicontinuous convex functions, and let $L_{k,i}: \mathcal{H}_i \rightarrow \mathcal{G}_k$ be a linear operator. The objective is to

$$\underset{x_1 \in \mathcal{H}_1, \dots, x_m \in \mathcal{H}_m}{\text{minimize}} \quad \underbrace{\sum_{i=1}^m f_i(x_i)}_{\text{separable term}} + \underbrace{\sum_{k=1}^p g_k \left(\sum_{i=1}^m L_{k,i} x_i \right)}_{k\text{th coupling term}}. \quad (1)$$

We denote the solution set by \mathcal{P} .

To solve Problem 1 reliably without adding restrictions on its constituents (for instance smoothness or strong convexity of some functions involved in the model), we focus on algorithms that have the following flexible features:

- ① **Nondifferentiability:** None of the functions $f_1, \dots, f_m, g_1, \dots, g_p$ is assumed to be differentiable.
- ② **Splitting:** The functions $f_1, \dots, f_m, g_1, \dots, g_p$ and the linear operators are activated separately.
- ③ **Block activation:** As m and p can be very large, only a block of the proximity operators of the functions $f_1, \dots, f_m, g_1, \dots, g_p$ is activated at each iteration.
- ④ **Operator norms:** Bounds on the norms of the linear operators involved in Problem 1 are not assumed.
- ⑤ **Convergence:** The algorithm produces a sequence which converges (possibly almost surely) to a solution to (1).

A consequence of features ① and ② is that the algorithms under consideration must activate the functions $f_1, \dots, f_m, g_1, \dots, g_p$ via their respective proximity operators (even if some functions happened to be smooth, proximal activation is often preferable [6, 11]). Feature ③ has a view towards current large-scale problems. In such scenarios, memory and computing power limitations make the execution of standard proximal splitting algorithms, which require activating all the proximity operators at each iteration, inefficient or simply impossible. As a result, we must turn our attention to algorithms which employ, at each iteration n , only blocks of functions $(f_i)_{i \in I_n}$ and $(g_k)_{k \in K_n}$. If the functions $(g_k)_{1 \leq k \leq p}$ were all smooth, one could use block-activated versions of the forward-backward algorithm proposed in [16, 25] and the references therein; in particular,

when $m = 1$, methods such as those of [12, 18, 23, 26] would be pertinent. Next, as noted in [16, Remark 5.10(iv)], another candidate of interest could be the randomly block-activated algorithm of [16, Section 5.2], which leads to block-activated versions of several primal-dual methods (see [24] for detailed developments and [8] for an inertial version when $m = 1$). However, this approach violates requirement ④ because it imposes bounds on the proximal scaling parameters which depend on the norms of the linear operators. Finally, requirement ⑤ rules out methods that guarantee merely minimizing sequences or ergodic convergence.

To the best of our knowledge, there seems to be two primary methods that fulfill ①–⑤:

- Algorithm **A**: The stochastic primal-dual Douglas–Rachford algorithm of [16].
- Algorithm **B**: The deterministic primal-dual projective splitting algorithm of [10].

In the case of smooth coupling functions $(g_k)_{1 \leq k \leq p}$, extensive numerical experience has been accumulated to understand the behavior of block-activated methods, especially in the case of stochastic gradient methods. By contrast, to date, very few numerical experiments with the recent, fully nonsmooth Algorithms **A** and **B** have been conducted and no comparison of their merits and performance has been undertaken. Thus far, Algorithm **A** has been employed only in the context of machine learning (see also the variant for partially smooth problems proposed in [6]). On the other hand, Algorithm **B** has been used in image recovery in [11], but only in full activation mode, and in rare feature selection in [22], but with $m = 1$.

Objectives: This paper aims at filling the above gap by shedding light on the implementation, the features, and the behavior of the fully nonsmooth Algorithms **A** and **B**, comparing their merits, and providing numerical experiments illustrating their performance.

Contributions and outline: In Section 2, we illustrate the pertinence and the versatility of the model proposed in Problem 1 through a panel of examples drawn from various fields. Algorithms **A** and **B** are presented in Section 3, where we analyze and compare their features, implementation, and asymptotic properties. This investigation is complemented in Section 4 by numerical experiments in the context of machine learning and image recovery.

2 Instantiations of Problem 1

We illustrate the pertinence and the versatility of the proposed model through a few examples.

Example 2 Variational models in multispectral imaging naturally involve minimization over several components. Specific references are [4, 7].

Example 3 In perspective maximum-likelihood type estimation, the goal is to estimate scale vectors $s = (\sigma_i)_{1 \leq i \leq N}$ and $t = (\tau_i)_{1 \leq i \leq P}$, as well as a regression vector $b \in \mathbb{R}^d$ [14]. The minimization problem assumes the form

$$\underset{s \in \mathbb{R}^N, t \in \mathbb{R}^P, b \in \mathbb{R}^d}{\text{minimize}} \quad \varsigma(s) + \varpi(t) + \theta(b) + \sum_{i=1}^N \Phi_i(\sigma_i, X_i b) + \sum_{i=1}^P \Psi_i(\tau_i, L_i b), \quad (2)$$

where all the functions are convex, (X_1, \dots, X_N) are design matrices, and (L_1, \dots, L_P) are linear transformations.

Example 4 We consider the latent group lasso formulation in machine learning [21]. Let $\{p_1, \dots, p_m\} \subset [1, +\infty]$, let $\{G_1, \dots, G_m\}$ be a covering of $\{1, \dots, d\}$, and define

$$X = \{(x_1, \dots, x_m) \mid x_i \in \mathbb{R}^d, \text{support}(x_i) \subset G_i\}. \quad (3)$$

The solution is $\tilde{y} = \sum_{i=1}^m \tilde{x}_i$, where $(\tilde{x}_1, \dots, \tilde{x}_m)$ solves

$$\underset{(x_1, \dots, x_m) \in X}{\text{minimize}} \quad \sum_{i=1}^m \tau_i \|x_i\|_{p_i} + \sum_{k=1}^p g_k \left(\sum_{i=1}^m \langle x_i \mid u_k \rangle \right), \quad (4)$$

with $\tau_i \in]0, +\infty[$, $u_k \in \mathbb{R}^d$, and $g_k: \mathbb{R} \rightarrow]-\infty, +\infty]$ convex.

Example 5 Various signal recovery problems can be modeled as infimal convolution problems of the form

$$\underset{x \in \mathcal{H}}{\text{minimize}} \quad f(x) + \sum_{k=1}^p (f_k \square g_k)(L_k x), \quad (5)$$

where all the functions are convex, $L_k: \mathcal{H} \rightarrow \mathcal{G}_k$ is linear, and \square is the inf-convolution operation, e.g., [2, 11, 20]. Under mild conditions, (5) can be rephrased as

$$\underset{\substack{x \in \mathcal{H} \\ y_1 \in \mathcal{G}_1, \dots, y_p \in \mathcal{G}_p}}{\text{minimize}} \quad f(x) + \sum_{k=1}^p f_k(y_k) + \sum_{k=1}^p g_k(L_k x - y_k). \quad (6)$$

3 Algorithms: Presentation and discussion

The subdifferential, the conjugate, and the proximity operator of a proper lower semicontinuous convex function $f: \mathcal{H} \rightarrow]-\infty, +\infty]$ are denoted by ∂f , f^* , and prox_f , respectively. Let us consider the setting of Problem 1 and let us set $\mathcal{H} = \mathcal{H}_1 \times \dots \times \mathcal{H}_m$ and $\mathcal{G} = \mathcal{G}_1 \times \dots \times \mathcal{G}_p$. A generic element in \mathcal{H} is denoted by $x = (x_i)_{1 \leq i \leq m}$. We make the standing assumption that the Kuhn–Tucker set of Problem 1 is nonempty, that is, there exist $\tilde{x} \in \mathcal{H}$ and $\tilde{v}^* \in \mathcal{G}$ such that

$$\begin{cases} (\forall i \in \{1, \dots, m\}) \quad -\sum_{k=1}^p L_{k,i}^* \tilde{v}_k^* \in \partial f_i(\tilde{x}_i) \\ (\forall k \in \{1, \dots, p\}) \quad \sum_{i=1}^m L_{k,i} \tilde{x}_i \in \partial g_k^*(\tilde{v}_k^*). \end{cases} \quad (7)$$

This implies that the solution set \mathcal{P} of Problem 1 is nonempty.

As discussed in Section 1, two primary algorithms seem to fulfill requirements ①–⑤. The first algorithm operates in the product space $\mathcal{H} \times \mathcal{G}$ and employs random activation of the blocks. To present it, let us introduce

$$\mathbf{L}: \mathcal{H} \rightarrow \mathcal{G}: x \mapsto \left(\sum_{i=1}^m L_{1,i} x_i, \dots, \sum_{i=1}^m L_{p,i} x_i \right) \quad (8)$$

and

$$\mathbf{V} = \{(\mathbf{z}, \mathbf{y}) \in \mathcal{H} \times \mathcal{G} \mid \mathbf{y} = \mathbf{Lz}\}. \quad (9)$$

Let $\mathbf{z} \in \mathcal{H}$ and $\mathbf{y} \in \mathcal{G}$, and set $\mathbf{t} = (\mathbf{Id} + \mathbf{L}^* \mathbf{L})^{-1}(\mathbf{z} + \mathbf{L}^* \mathbf{y})$ and $\mathbf{s} = (\mathbf{Id} + \mathbf{L} \mathbf{L}^*)^{-1}(\mathbf{L} \mathbf{z} - \mathbf{y})$. Then the projection of $(\mathbf{z}, \mathbf{y}) \in \mathcal{H} \times \mathcal{G}$ onto \mathbf{V} is [16, Eq. (5.25)]

$$\text{proj}_{\mathbf{V}}(\mathbf{z}, \mathbf{y}) = (\mathbf{t}, \mathbf{L} \mathbf{t}) = (\mathbf{z} - \mathbf{L}^* \mathbf{s}, \mathbf{y} + \mathbf{s}). \quad (10)$$

The coordinate operators of $\text{proj}_{\mathbf{V}}$ are $(Q_j)_{1 \leq j \leq m+p}$, i.e.,

$$\text{proj}_{\mathbf{V}}(\mathbf{z}, \mathbf{y}) = (Q_1(\mathbf{z}, \mathbf{y}), \dots, Q_{m+p}(\mathbf{z}, \mathbf{y})). \quad (11)$$

Algorithm A ([16]) Let $\gamma \in]0, +\infty[$, let \mathbf{x}_0 and \mathbf{z}_0 be \mathcal{H} -valued random variables (r.v.), let \mathbf{y}_0 and \mathbf{w}_0 be \mathcal{G} -valued r.v. Iterate

```

for  $j = 1, \dots, m + p$ 
| compute  $Q_j$  given by (8)–(11)
for  $n = 0, 1, \dots$ 
|  $\lambda_n \in ]0, 2[$ 
| select randomly  $\emptyset \neq I_n \subset \{1, \dots, m\}$  and  $\emptyset \neq K_n \subset \{1, \dots, p\}$ 
| for every  $i \in I_n$ 
| |  $x_{i,n+1} = Q_i(\mathbf{z}_n, \mathbf{y}_n)$ 
| |  $z_{i,n+1} = z_{i,n} + \lambda_n(\text{prox}_{\gamma f_i}(2x_{i,n+1} - z_{i,n}) - x_{i,n+1})$ 
| for every  $i \in \{1, \dots, m\} \setminus I_n$ 
| |  $(x_{i,n+1}, z_{i,n+1}) = (x_{i,n}, z_{i,n})$ 
| for every  $k \in K_n$ 
| |  $w_{k,n+1} = Q_{m+k}(\mathbf{z}_n, \mathbf{y}_n)$ 
| |  $y_{k,n+1} = y_{k,n} + \lambda_n(\text{prox}_{\gamma g_k}(2w_{k,n+1} - y_{k,n}) - w_{k,n+1})$ 
| for every  $k \in \{1, \dots, p\} \setminus K_n$ 
| |  $(w_{k,n+1}, y_{k,n+1}) = (w_{k,n}, y_{k,n}).$ 

```

Theorem 6 ([16]) In the setting of Algorithm A, define, for every $n \in \mathbb{N}$ and every $j \in \{1, \dots, m + p\}$,

$$\varepsilon_{j,n} = \begin{cases} 1, & \text{if } j \in I_n \text{ or } j - m \in K_n; \\ 0, & \text{otherwise.} \end{cases} \quad (13)$$

Suppose that the following hold:

- [a] $\inf_{n \in \mathbb{N}} \lambda_n > 0$ and $\sup_{n \in \mathbb{N}} \lambda_n < 2$.
- [b] The r.v. $(\varepsilon_n)_{n \in \mathbb{N}}$ are identically distributed.
- [c] For every $n \in \mathbb{N}$, the r.v. ε_n and $(\mathbf{z}_j, \mathbf{y}_j)_{0 \leq j \leq n}$ are mutually independent.
- [d] $(\forall j \in \{1, \dots, m + p\}) \text{Prob}[\varepsilon_{j,0} = 1] > 0$.

Then $(\mathbf{x}_n)_{n \in \mathbb{N}}$ converges almost surely to a \mathcal{P} -valued r.v.

The second algorithm operates by projecting onto hyperplanes which separate the current iterate from the Kuhn–Tucker set of Problem 1 and activating the blocks in a deterministic manner [10].

Algorithm B ([10]) Set $I_0 = \{1, \dots, m\}$ and $K_0 = \{1, \dots, p\}$. For every $i \in \{1, \dots, m\}$ and every $k \in \{1, \dots, p\}$, let $\{\gamma_i, \mu_k\} \subset]0, +\infty[$, $x_{i,0} \in \mathcal{H}_i$, and $v_{k,0}^* \in \mathcal{G}_k$. Iterate

```

for  $n = 0, 1, \dots$ 
   $\lambda_n \in ]0, 2[$ 
  if  $n > 0$ 
    | select  $\emptyset \neq I_n \subset \{1, \dots, m\}$  and  $\emptyset \neq K_n \subset \{1, \dots, p\}$ 
    for every  $i \in I_n$ 
      |  $x_{i,n}^* = x_{i,n} - \gamma_i \sum_{k=1}^p L_{k,i}^* v_{k,n}^*$ 
      |  $a_{i,n} = \text{prox}_{\gamma_i f_i} x_{i,n}^*$ 
      |  $a_{i,n}^* = \gamma_i^{-1} (x_{i,n}^* - a_{i,n})$ 
    for every  $i \in \{1, \dots, m\} \setminus I_n$ 
      |  $(a_{i,n}, a_{i,n}^*) = (a_{i,n-1}, a_{i,n-1}^*)$ 
    for every  $k \in K_n$ 
      |  $y_{k,n}^* = \mu_k v_{k,n}^* + \sum_{i=1}^m L_{k,i} x_{i,n}$ 
      |  $b_{k,n} = \text{prox}_{\mu_k g_k} y_{k,n}^*$ 
      |  $b_{k,n}^* = \mu_k^{-1} (y_{k,n}^* - b_{k,n})$ 
      |  $t_{k,n} = b_{k,n} - \sum_{i=1}^m L_{k,i} a_{i,n}$ 
    for every  $k \in \{1, \dots, p\} \setminus K_n$ 
      |  $(b_{k,n}, b_{k,n}^*) = (b_{k,n-1}, b_{k,n-1}^*)$ 
      |  $t_{k,n} = b_{k,n} - \sum_{i=1}^m L_{k,i} a_{i,n}$ 
    for every  $i \in \{1, \dots, m\}$ 
      |  $t_{i,n}^* = a_{i,n}^* + \sum_{k=1}^p L_{k,i}^* b_{k,n}^*$ 
     $\tau_n = \sum_{i=1}^m \|t_{i,n}^*\|^2 + \sum_{k=1}^p \|t_{k,n}\|^2$ 
    if  $\tau_n > 0$ 
      |  $\pi_n = \sum_{i=1}^m (\langle x_{i,n} \mid t_{i,n}^* \rangle - \langle a_{i,n} \mid a_{i,n}^* \rangle) + \sum_{k=1}^p (\langle t_{k,n} \mid v_{k,n}^* \rangle - \langle b_{k,n} \mid b_{k,n}^* \rangle)$ 
    if  $\tau_n > 0$  and  $\pi_n > 0$ 
      |  $\theta_n = \lambda_n \pi_n / \tau_n$ 
      | for every  $i \in \{1, \dots, m\}$ 
        | |  $x_{i,n+1} = x_{i,n} - \theta_n t_{i,n}^*$ 
      | for every  $k \in \{1, \dots, p\}$ 
        | |  $v_{k,n+1}^* = v_{k,n}^* - \theta_n t_{k,n}$ 
    else
      | for every  $i \in \{1, \dots, m\}$ 
        | |  $x_{i,n+1} = x_{i,n}$ 
      | for every  $k \in \{1, \dots, p\}$ 
        | |  $v_{k,n+1}^* = v_{k,n}^*$ .
  
```

(14)

Theorem 7 ([10]) In the setting of Algorithm B, suppose that the following hold:

- [a] $\inf_{n \in \mathbb{N}} \lambda_n > 0$ and $\sup_{n \in \mathbb{N}} \lambda_n < 2$.
- [b] There exists $T \in \mathbb{N}$ such that, for every $n \in \mathbb{N}$, $\bigcup_{j=n}^{n+T} I_j = \{1, \dots, m\}$ and $\bigcup_{j=n}^{n+T} K_j = \{1, \dots, p\}$.

Then $(x_n)_{n \in \mathbb{N}}$ converges to a point in \mathcal{P} .

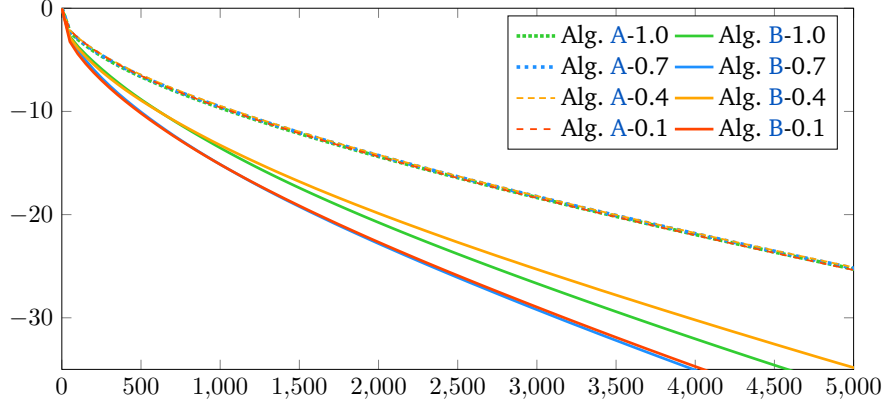


Figure 1: Normalized error $20 \log_{10}(\|x_n - x_\infty\|/\|x_0 - x_\infty\|)$ (dB), averaged over 20 runs, versus epoch count in Experiment 1. The variations around the averages were not significant. The computational load per epoch for both algorithms is comparable.

Remark 8 (comparing Algorithms A and B)

- (i) **Auxiliary tasks:** Algorithm A requires the construction and storage of the operators $(Q_j)_{1 \leq j \leq m+p}$ of (10)–(11), which can be quite demanding as they involve inversion of a linear operator acting on the product space \mathcal{H} or \mathcal{G} . By contrast, Algorithm B does not require such tasks.
- (ii) **Proximity operators:** In both algorithms, only the proximity operators of the blocks of functions $(f_i)_{i \in I_n}$ and $(g_k)_{k \in K_n}$ need to be activated at iteration n .
- (iii) **Linear operators:** In Algorithm A, the operators $(Q_i)_{i \in I_n}$ and $(Q_{m+k})_{k \in K_n}$ selected at iteration n are evaluated at $(z_{1,n}, \dots, z_{m,n}, y_{1,n}, \dots, y_{p,n}) \in \mathcal{H} \times \mathcal{G}$. On the other hand, Algorithm B activates the local operators $L_{k,i}: \mathcal{H}_i \rightarrow \mathcal{G}_k$ and $L_{k,i}^*: \mathcal{G}_k \rightarrow \mathcal{H}_i$ once or twice, depending on whether they are selected. For instance, if we set $N = \dim \mathcal{H}$ and $M = \dim \mathcal{G}$ and if all the linear operators are implemented in matrix form, then the corresponding load per iteration in full activation mode of Algorithm A is $\mathcal{O}((M + N)^2)$ versus $\mathcal{O}(MN)$ in Algorithm B.
- (iv) **Activation scheme:** As Algorithm A selects the blocks randomly, the user does not have complete control of the computational load of an iteration, whereas that of Algorithm B is more predictable because of its deterministic activation scheme.
- (v) **Parameters:** A single scale parameter γ is used in Algorithm A, while Algorithm B allows the proximity operators to have their own scale parameters $(\gamma_1, \dots, \gamma_m, \mu_1, \dots, \mu_p)$. This gives Algorithm B more flexibility, but more effort may be needed to find efficient parameters. Furthermore, in both algorithms, there is no restriction on the parameter values.
- (vi) **Convergence:** Algorithm B guarantees sure convergence under the mild sweeping condition [b] in Theorem 7, while A guarantees only almost sure convergence.
- (vii) **Other features:** Although this point is omitted for brevity, unlike Algorithm A, Algorithm B can be executed asynchronously with iteration-dependent scale parameters [10].

4 Numerical experiments

We present two experiments which are reflective of our numerical investigations in solving various problems using Algorithms A and B.

4.1 Experiment 1: Group-sparse binary classification

We revisit the problem from [13], which is set as Example 4 with $g_k: \xi \mapsto \max\{0, 1 - \beta_k \xi\}$, where $\beta_k = \omega_k \operatorname{sign}(\langle \bar{y} \mid u_k \rangle)$ is the k th measurement of the true vector $\bar{y} \in \mathbb{R}^d$ ($d = 10000$) and $\omega_k \in \{-1, 1\}$ induces 25% classification error. There are $p = 1000$ measurements and the goal is to reconstruct the group-sparse vector \bar{y} . There are $m = 1429$ groups. For every $i \in \{1, \dots, m-1\}$, each G_i has 10 consecutive integers and an overlap with G_{i+1} of length 3. We obtain an instance of (1), where $\mathcal{H}_i = \mathbb{R}^{10}$, $f_i = 0.1 \|\cdot\|_2$, and $L_{k,i} = \langle \cdot \mid u_k|_{G_i} \rangle$. The auxiliary tasks for Algorithm A (see Remark 8(i)) are negligible [13]. For each $\alpha \in \{0.1, 0.4, 0.7, 1.0\}$, at iteration $n \in \mathbb{N}$, I_n has $\lceil \alpha m \rceil$ elements and the proximity operators of the scalar functions $(g_k)_{1 \leq k \leq p}$ are all used, i.e., $K_n = \{1, \dots, p\}$. We display in Fig. 1 the normalized error versus the epoch, that is, the cumulative number of activated blocks in $\{1, \dots, m\}$ divided by m .

4.2 Experiment 2: Image recovery

We revisit the image interpolation problem from [11, Section 4.3]. The objective is to recover the image $\bar{x} \in C = [0, 255]^N$ ($N = 96^2$) of Fig. 2(a), given a noisy masked observation $b = M\bar{x} + w_1 \in \mathbb{R}^N$ and a noisy blurred observation $c = H\bar{x} + w_2 \in \mathbb{R}^N$. Here, M masks all but $q = 39$ rows $(x^{(r_k)})_{1 \leq k \leq q}$ of an image x , and H is a nonstationary blurring operator, while w_1 and w_2 yield signal-to-noise ratios of 28.5 dB and 27.8 dB, respectively. Since H is sizable, we split it into $s = 384$ subblocks: for every $k \in \{1, \dots, s\}$, $H_k \in \mathbb{R}^{24 \times N}$ and the corresponding block of c is denoted c_k . The goal is to

$$\underset{x \in C}{\text{minimize}} \quad \|Dx\|_{1,2} + 10 \sum_{k=1}^q \|x^{(r_k)} - b^{(r_k)}\|_2 + 5 \sum_{k=1}^s \|H_k x - c_k\|_2^2, \quad (15)$$

where $D: \mathbb{R}^N \rightarrow \mathbb{R}^N \times \mathbb{R}^N$ models finite differences and $\|\cdot\|_{1,2}: (y_1, y_2) \mapsto \sum_{j=1}^N \|(\eta_{1,j}, \eta_{2,j})\|_2$. Thus, (15) is an instance of Problem 1, where $m = 1$; $p = q + s + 1$; for every $k \in \{1, \dots, q\}$, $L_{k,1}: \mathbb{R}^N \rightarrow \mathbb{R}^{\sqrt{N}}: x \mapsto x^{(r_k)}$ and $g_k: y_k \mapsto 10\|y_k - b^{(r_k)}\|_2$; for every $k \in \{q + 1, \dots, q + s\}$, $L_{k,1} = H_{k-q}$, $g_k = 5\|\cdot - c_k\|_2^2$, and $g_p = \|\cdot\|_{1,2}$; $L_{p,1} = D$; $f_1: x \mapsto 0$ if $x \in C$; $+\infty$ if $x \notin C$. At iteration n , K_n has $\lceil \alpha p \rceil$ elements, where $\alpha \in \{0.1, 0.4, 0.7, 1.0\}$. The results are shown in Figs. 2–3, where the epoch is the cumulative number of activated blocks in $\{1, \dots, p\}$ divided by p .

4.3 Discussion

Our first finding is that, for both Algorithms A and B, even when full activation is possible, it may not be the best strategy (see Figs. 1 and 3). Second, Remark 8 and our experiments strongly suggest that Algorithm B may be preferable to A. Let us add that, in general, Algorithm A does not scale as well as B. For instance, in Experiment 2, if the image size scales up, Algorithm B can still

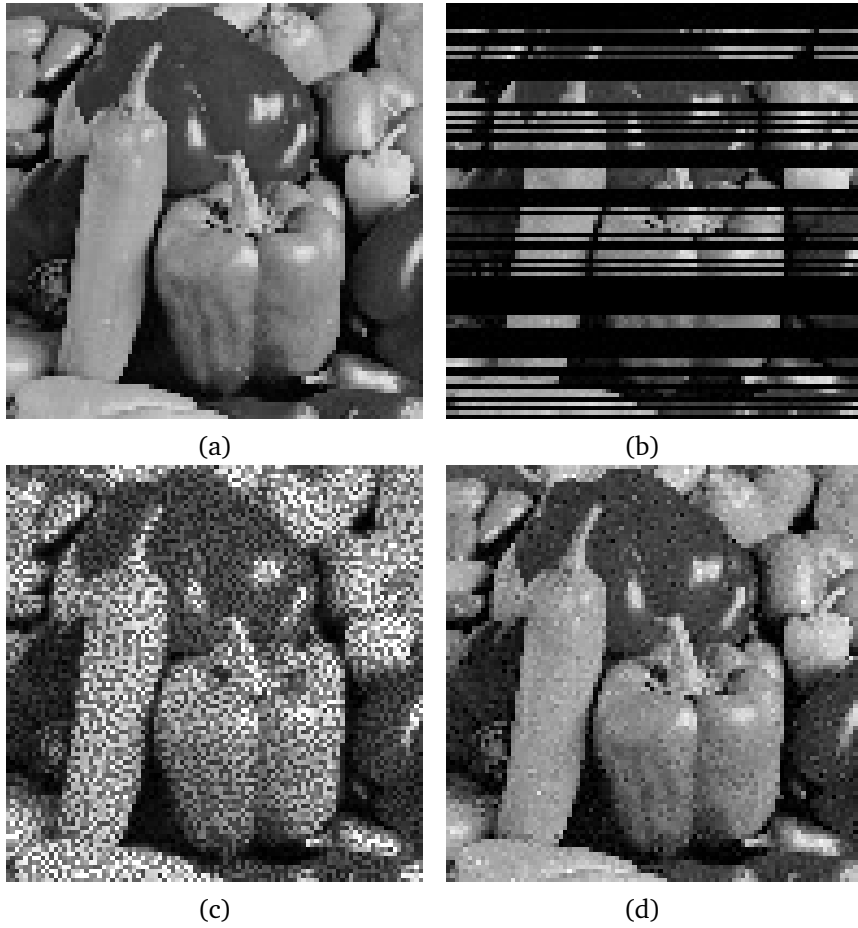


Figure 2: Experiment 2: (a) Original \bar{x} . (b) Observation b . (c) Observation c . (d) Recovery (all recoveries were visually indistinguishable).

operate since it involves only individual applications of the local $L_{k,i}$ operators, while Algorithm A becomes unmanageable because of the size of the Q_j operators (see Remark 8(i) and [6]).

Per Remark 8(vii), we are currently exploring the numerical benefits of implementing Algorithm B asynchronously.

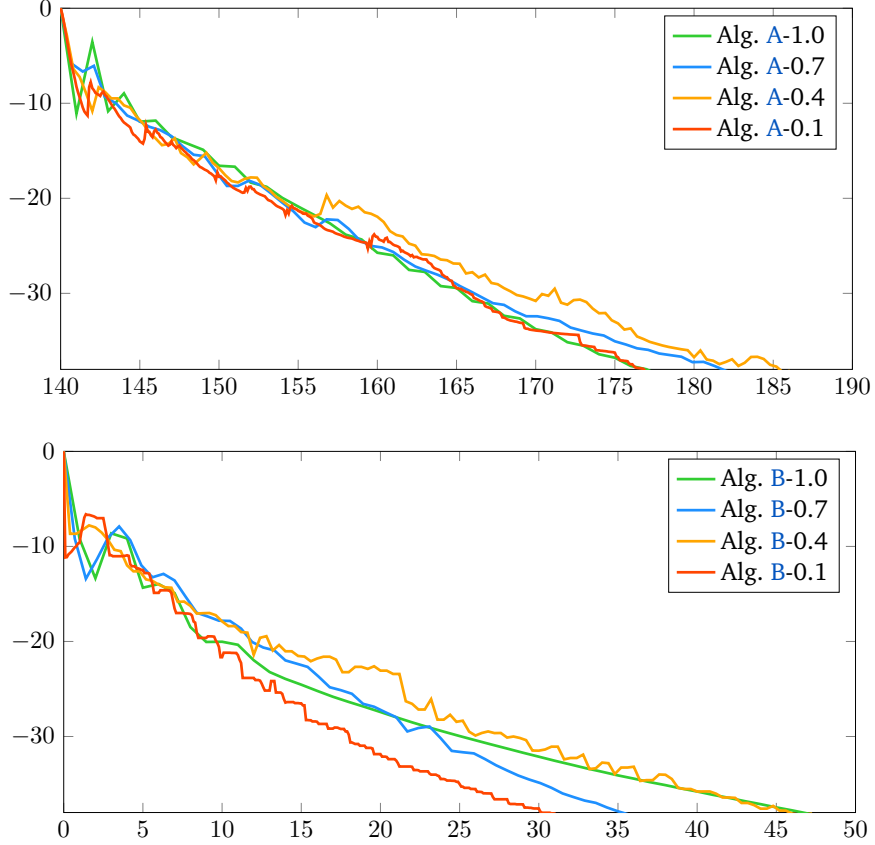


Figure 3: Normalized error $20 \log_{10}(\|x_n - x_\infty\|/\|x_0 - x_\infty\|)$ (dB) versus epoch count in Experiment 2. Top: Algorithm A. The horizontal axis starts at 140 epochs to account for the auxiliary tasks (see Remark 8(i)). Bottom: Algorithm B. The computational load per epoch for Algorithm B was about twice that of Algorithm A.

References

- [1] A. Argyriou, R. Foygel, and N. Srebro, Sparse prediction with the k -support norm, *Proc. Adv. Neural Inform. Process. Syst. Conf.*, vol. 25, pp. 1457–1465, 2012.
- [2] J.-F. Aujol and A. Chambolle, Dual norms and image decomposition models, *Int. J. Comput. Vision*, vol. 63, pp. 85–104, 2005.
- [3] F. Bach, R. Jenatton, J. Mairal, and G. Obozinski, Optimization with sparsity-inducing penalties, *Found. Trends Machine Learn.*, vol. 4, pp. 1–106, 2012.
- [4] J. M. Bioucas-Dias, A. Plaza, N. Dobigeon, M. Parente, Q. Du, P. Gader, and J. Chanussot, Hyperspectral unmixing overview: Geometrical, statistical, and sparse regression-based approaches, *IEEE J. Select. Topics Appl. Earth Observ. Remote Sensing*, vol. 5, pp. 354–379, 2012.
- [5] S. Boyd, N. Parikh, E. Chu, B. Peleato, and J. Eckstein, Distributed optimization and statistical learning via the alternating direction method of multipliers, *Found. Trends Machine Learn.*, vol. 3, pp. 1–122, 2010.
- [6] L. M. Briceño-Arias, G. Chierchia, E. Chouzenoux, and J.-C. Pesquet, A random block-coordinate Douglas-Rachford splitting method with low computational complexity for binary logistic regression, *Comput. Optim. Appl.*, vol. 72, pp. 707–726, 2019.

- [7] L. M. Briceño-Arias, P. L. Combettes, J.-C. Pesquet, and N. Pustelnik, Proximal algorithms for multi-component image recovery problems, *J. Math. Imaging Vision*, vol. 41, pp. 3–22, 2011.
- [8] A. Chambolle, M. J. Ehrhardt, P. Richtárik, and C.-B. Schönlieb, Stochastic primal-dual hybrid gradient algorithm with arbitrary sampling and imaging applications, *SIAM J. Optim.*, vol. 28, pp. 2783–2808, 2018.
- [9] A. Chambolle and T. Pock, An introduction to continuous optimization for imaging, *Acta Numer.*, vol. 25, pp. 161–319, 2016.
- [10] P. L. Combettes and J. Eckstein, Asynchronous block-iterative primal-dual decomposition methods for monotone inclusions, *Math. Program.*, vol. B168, pp. 645–672, 2018.
- [11] P. L. Combettes and L. E. Glaudin, Proximal activation of smooth functions in splitting algorithms for convex image recovery, *SIAM J. Imaging Sci.*, vol. 12, pp. 1905–1935, 2019.
- [12] P. L. Combettes and L. E. Glaudin, Solving composite fixed point problems with block updates, *Adv. Nonlinear Anal.*, vol. 10, 2021.
- [13] P. L. Combettes, A. M. McDonald, C. A. Micchelli, and M. Pontil, Learning with optimal interpolation norms, *Numer. Algorithms*, vol. 81, pp. 695–717, 2019.
- [14] P. L. Combettes and C. L. Müller, Perspective maximum likelihood-type estimation via proximal decomposition, *Electron. J. Stat.*, vol. 14, pp. 207–238, 2020.
- [15] P. L. Combettes and J.-C. Pesquet, Proximal splitting methods in signal processing, *Fixed-Point Algorithms for Inverse Problems in Science and Engineering*, pp. 185–212. Springer, 2011.
- [16] P. L. Combettes and J.-C. Pesquet, Stochastic quasi-Fejér block-coordinate fixed point iterations with random sweeping, *SIAM J. Optim.*, vol. 25, pp. 1221–1248, 2015.
- [17] J. Darbon and T. Meng, On decomposition models in imaging sciences and multi-time Hamilton–Jacobi partial differential equations, *SIAM J. Imaging Sci.*, vol. 13, pp. 971–1014, 2020.
- [18] A. J. Defazio, T. S. Caetano, and J. Domke, Finito: A faster, permutable incremental gradient method for big data problems, *Proc. Intl. Conf. Machine Learn.*, pp. 1125–1133, 2014.
- [19] R. Glowinski, S. J. Osher, and W. Yin (Eds.), *Splitting Methods in Communication, Imaging, Science, and Engineering*. Springer, 2016.
- [20] M. Hintermüller and G. Stadler, An infeasible primal-dual algorithm for total bounded variation-based inf-convolution-type image restoration, *SIAM J. Sci. Comput.*, vol. 28, pp. 1–23, 2006.
- [21] L. Jacob, G. Obozinski, and J.-Ph. Vert, Group lasso with overlap and graph lasso, *Proc. Int. Conf. Machine Learn.*, pp. 433–440, 2009.
- [22] P. R. Johnstone and J. Eckstein, Projective splitting with forward steps, *Math. Program.*, published online 2020-09-30.
- [23] K. Mishchenko, F. Iutzeler, and J. Malick, A distributed flexible delay-tolerant proximal gradient algorithm, *SIAM J. Optim.*, vol. 30, pp. 933–959, 2020.
- [24] J.-C. Pesquet and A. Repetti, A class of randomized primal-dual algorithms for distributed optimization, *J. Nonlinear Convex Anal.*, vol. 16, pp. 2453–2490, 2015.
- [25] S. Salzo and S. Villa, Parallel random block-coordinate forward-backward algorithm: A unified convergence analysis, *Math. Program.*, to appear.
- [26] M. Schmidt, N. Le Roux, and F. Bach, Minimizing finite sums with the stochastic average gradient, *Math. Program.*, vol. 162, pp. 83–112, 2017.